NLRP3 inflammasome mediates abnormal epithelial regeneration and distal lung remodeling in silica-induced lung fibrosis

HONG ZHOU[1], QUN ZHANG[2], CHENYANG LIU[2], JIAHAO FAN[2], WEN HUANG[2], NAN LI[2], MINGXIA YANG[3], HONG WANG[2], WEIPING XIE[2] and HUI KONG[2]

[1]Department of Pulmonary and Critical Care Medicine, The Affiliated Wuxi People's Hospital of Nanjing Medical University, Wuxi People's Hospital, Wuxi Medical Center, Nanjing Medical University, Wuxi, Jiangsu 214023; [2]Department of Pulmonary and Critical Care Medicine, The First Affiliated Hospital of Nanjing Medical University, Nanjing, Jiangsu 210029; [3]Department of Pulmonary and Critical Care Medicine, The Affiliated Changzhou No. 2 People's Hospital of Nanjing Medical University, Changzhou, Jiangsu 213003, P.R. China

Received September 6, 2023; Accepted December 28, 2023

DOI: 10.3892/ijmm.2024.5349

Abstract. NOD-like receptor protein 3 (NLRP3) inflammasome is closely related to silica particle-induced chronic lung inflammation but its role in epithelial remodeling, repair and regeneration in the distal lung during development of silicosis remains to be elucidated. The present study aimed to determine the effects of the NLRP3 inflammasome on epithelial remodeling and cellular regeneration and potential mechanisms in the distal lung of silica-treated mice at three time points. Pulmonary function assessment, inflammatory cell counting, enzyme-linked immunosorbent assay, histological and immunological analyses, hydroxyproline assay and western blotting were used in the study. Single intratracheal instillation of a silica suspension caused sustained NLRP3 inflammasome activation in the distal lung. Moreover, a time-dependent increase in airway resistance and a decrease in lung compliance accompanied progression of pulmonary fibrosis. In the terminal bronchiole, lung remodeling including pyroptosis (membrane-distributed GSDMD$^+$), excessive proliferation (Ki67$^+$), mucus overproduction (mucin 5 subtype AC and B) and epithelial-mesenchymal transition (decreased E-Cadherin$^+$ and increased Vimentin$^+$), was observed by immunofluorescence analysis. Notably, aberrant spatiotemporal expression of the embryonic lung stem/progenitor cell markers SOX2 and SOX9 and ectopic distribution of bronchioalveolar stem cells were observed in the distal lung only on the 7th day after silica instillation (the early inflammatory phase of silicosis). Western blotting revealed that the Sonic hedgehog/Glioma-associated oncogene (Shh/Gli) and Wnt/β-catenin pathways were involved in NLRP3 inflammasome activation-mediated epithelial remodeling and dysregulated regeneration during the inflammatory and fibrotic phases. Overall, sustained NLRP3 inflammasome activation led to epithelial remodeling in the distal lung of mice. Moreover, understanding the spatiotemporal profile of dysregulated epithelial repair and regeneration may provide a novel therapeutic strategy for inhalable particle-related chronic inflammatory and fibrotic lung disease.

Correspondence to: Professor Hui Kong or Professor Weiping Xie, Department of Pulmonary and Critical Care Medicine, The First Affiliated Hospital of Nanjing Medical University, 300 Guangzhou Road, Nanjing, Jiangsu 210029, P.R. China
E-mail: konghui@njmu.edu.cn
E-mail: wpxie@njmu.edu.cn

Key words: NLRP3 inflammasome, bronchoalveolar duct junction, bronchioalveolar stem cell, lung remodeling, repair, regeneration

Introduction

Chronic lung inflammation induced by inhalable particles is a major cause of chronic obstructive pulmonary disease (COPD), asthma, pulmonary fibrosis and occupational pulmonary diseases (1-3). Silicosis is an irreversible and incurable lung disease caused by inhalation of crystalline silica; even when patients are no longer exposed to silica particles, fibrosis continues to progress (4). Mounting evidence suggests that silica-induced persistent damage to the distal lung is a major cause of epithelial remodeling and fibrosis in silicosis (5) and epithelial remodeling is the final outcome caused by the functional abnormalities of epithelial cells, fibroblasts and immune cells (6,7). Histologically, inhaled silica particles are deposited in the terminal ends of distal bronchioles, contributing to mucous plugging (8), epithelial dysfunction (9,10) and peribronchiolar fibrosis and bronchiolar obstruction (11,12). Moreover, repetitive or recurrent injury to the distal lung results in dysregulated repair and regeneration, further promoting the development of pulmonary fibrosis (13,14).

The distal lung contains terminal bronchioles and alveoli that facilitate gas exchange and can be compromised by disorders including interstitial lung disease and coronavirus disease 2019 (15). The bronchoalveolar duct junction (BADJ) is a unique region at the terminal ends of distal bronchioles at which the lung is separated into the proximal conducting

airways and peripheral gas exchange region (16). At the BADJ, an abrupt transition occurs in cell type and morphology (airway to alveolar epithelial cells) (16), which determines the unique features and key roles of the area. Moreover, studies have demonstrated the importance of the BADJ as the niche for bronchioalveolar stem cells (BASCs) co-expressing markers of club cells and type II alveolar epithelial cells (17,18); this population exhibits a robust capacity for repair and regeneration when treated with naphthalene or bleomycin *in vivo* (19). Therefore, the distal lung is an appropriate site for study of reparative and regenerative responses in fibrotic lung injury.

The NLRP3 inflammasome is a large cytosolic protein complex comprising NLRP3, apoptosis-associated speck-like protein containing a CARD domain (ASC), and pro-Caspase-1 (20). Once activated, the assembled complex activates pro-Caspase-1; cleaved Caspase-1 in turn produces the biologically active forms of pro-interleukin-1β (IL-1β) and IL-18, as well as pyroptotic cell death (21,22). To date, the NLRP3 inflammasome has been demonstrated to contribute to the progression of several types of inflammatory respiratory disease, including lung fibrosis (23,24). Additionally, silica is a well-recognized activator of the NLRP3 inflammasome (25,26), which promotes inflammatory damage leading to progressive fibrosis in silicosis. MCC950 is a highly potent specific NLRP3 inhibitor with good pharmacokinetic and pharmacodynamic properties that can block NLRP3-mediated ASC oligomerization and inflammasome assembly (27,28). Additionally, inflammasome activation appears to regulate the balance between tissue repair and inflammation following inhalation of crystalline silica (29). However, it remains unclear whether silica-induced NLRP3 inflammasome activation mediates epithelial remodeling and dysregulated regeneration in the distal lung. In the present study, a silica-induced mouse lung fibrosis model was used to examine the effects and mechanisms of the NLRP3 inflammasome on regulating the balance between pulmonary inflammation, epithelial remodeling and dysregulated regeneration in the distal lung at three time points.

Materials and methods

Animals. All experimental procedures involving mice were approved by the Institutional Animal Care and Use Committee of Nanjing Medical University (Nanjing, China; approval no. NJMU/IACUC-2012034) and complied with the guidelines published by the National Institutes of Health Guide for the Care and Use of Laboratory Animals (NIH publication No. 85-23, revised 1996) (30). A total of 72 male C57BL/6 mice (22-25 g; age, 8 weeks) provided by Nanjing Medical University Experimental Animal Center (Nanjing, China) were given free access to food and water at 22˚C), controlled illumination (12 h light/dark cycles) and suitable humidity (40-60%).

Experimental design. After 1 week of acclimation to the environment, wild-type C57BL/6 mice were randomly assigned to four groups (normal saline, normal saline + MCC950, silica and silica + MCC950; n=18/group) and received a single tracheal instillation of 50 μl sterile saline or 2.5 mg silica crystals (cat. no. CAS14808-60-7; purity 99%; particle diameter 0.5-10.0 μm; Sigma-Aldrich; Merck KGaA) in the same volume of sterile saline. MCC950 (10 mg/kg; Selleck Chemicals) was administered intraperitoneally every day for the first 3 days and every other day for the next 4, 25 or 53 days. Sterile saline was intraperitoneally injected into mice as the negative control. Six mice from each group were anesthetized with an intraperitoneal injection of sodium pentobarbital (50 mg/kg) and sacrificed at 7, 28 and 56 days post-instillation (Fig. 1).

Assessment of pulmonary function. Prior to sacrifice of the mice, the Buxco FinePointe RC system (Data Sciences International) was used to analyze ventilatory parameters, including static lung compliance, dynamic lung compliance and airway resistance of mice. Respiratory frequency was set as 100 breaths/min and tidal volume was set as 0.2 ml with a positive end-expiratory pressure of 2 cm H_2O. The mean values (n=6) were recorded during 3-min period following ventilation.

Bronchoalveolar lavage fluid (BALF) collection and cell counting. BALF was collected after the mice were euthanized with an overdose of sodium pentobarbital (150 mg/kg). BALF was obtained by infusing 0.5 ml cold sterile saline three consecutive times with the assistance of tracheal cannulation, followed by centrifugation at 200 x g and 4˚C for 10 min. The supernatant was separated and stored at -80˚C for subsequent analysis, and the cell pellets were resuspended in 1 ml saline for differential cell counting using a BTX-1800 hematology analyzer (Zibo Hengtuo Analytical Instrument Co., Ltd.).

Analysis of IL-1β, IL-18, TNF-α and IL-10 in BALF. The levels of IL-1β (cat. no. KE10003, Proteintech), IL-18 (CSB-E04609m, CUSABIO), TNF-α (KE10002, Proteintech) and IL-10 (KE10008, Proteintech) in BALF were measured using enzyme-linked immunosorbent assay kits according to the manufacturer's instructions.

Histological, immunohistochemical and immunofluorescent analyses. Right lung tissue was infused with 4% (w/v) paraformaldehyde (Sigma-Aldrich; Merck KGaA) using a blunted 30-gauge needle through the trachea and fixed in 4% paraformaldehyde at 4˚C overnight.

For paraffin sectioning, the lungs were dehydrated using an ethanol gradient, embedded in paraffin and sectioned (5 μm). Hematoxylin and eosin (H&E) and Masson's trichrome staining were performed following standard protocols (31,32) and examined by an Olympus VS200 slide scanner (Olympus Corporation) to assess mean inflammation or fibrosis. Lung inflammation was graded as previously described (33): none (0), no alveolitis; mild (1+), affected area <20%; moderate (2+), affected area 20-50% and severe (3+), affected area >50%. Lung fibrosis was graded and quantified by the modified scale (34): alveolar septa: no fibrotic burden at the most flimsy small fibers in some alveolar walls, lung structure: normal lung (0); alveolar septa: isolated gentle fibrotic changes, lung structure: alveoli partly enlarged and rarefied, but no fibrotic masses present (1); alveolar septa: clearly fibrotic changes with knot-like formation but not connected to each other, lung structure: alveoli partly enlarged and rarefied but no fibrotic masses (2); alveolar septa: contiguous fibrotic walls

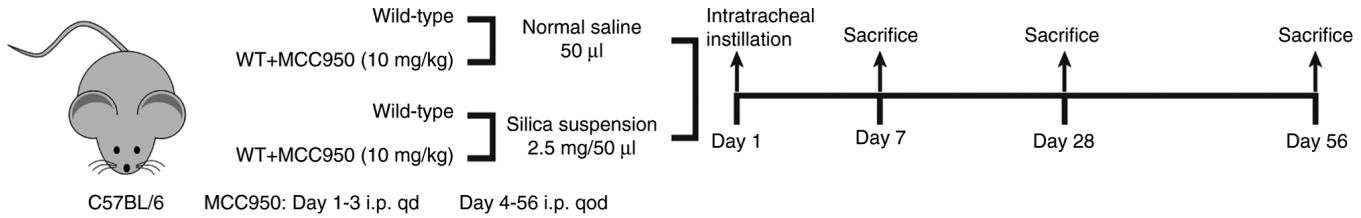

Figure 1. Schematic diagram of the experimental procedure involving the animal model. Male C57BL/6 mice received a single intratracheal instillation of a silica particle suspension (2.5 mg/50 μl) or vehicle. These mice received 200 μl 10 mg/kg MCC950 or control normal saline via i.p. injection qd for the first 3 days and qod for 53 consecutive days (27 injections). i.p., intraperitoneal; qd, once daily; qod, every other day.

predominantly in whole microscopic field, lung structure: alveoli partly enlarged and rarefied, but no fibrotic masses (3); alveolar septa: variable, lung structure: single fibrotic masses (4); alveolar septa: variable, lung structure: confluent fibrotic masses, and lung structure severely damaged but still preserved (5); alveolar septa: variable, mostly not existent, lung structure: large contiguous fibrotic masses, and lung architecture mostly not preserved (6); alveolar septa: non-existent, lung structure: alveoli nearly obliterated with fibrous masses but still up to five air bubbles (7); alveolar septa: non-existent, lung structure: microscopic field with complete obliteration with fibrotic masses (8). Immunostaining was performed using standard procedures. Briefly, paraffin sections were dewaxed using xylene and rehydrated using gradient alcohol, and antigen repair was performed by microwave heating (95˚C, 20 min). The sections were blocked with QuickBlock™ Blocking Buffer (Beyotime Institute of Biotechnology) for 30 min at room temperature and incubated at 4˚C overnight with anti-NLRP3 (1:50, cat. no. NBP2-12446, Novus Biologicals, LLC), anti-Caspase-1 (1:100; cat. no. ab138483, Abcam), anti-IL-1β (1:200, ab205924, Abcam), anti-Ki67 (1:200, AF0198, Affinity Biosciences), anti-surfactant protein C (SPC) (1:200, DF6647, Affinity Biosciences), anti-club cell 10 kDa protein (CC10) (1:200, sc-365992, Santa Cruz Biotechnology, Inc.), anti-gasdermin D (GSDMD) (1:400, AF4012, Affinity Biosciences), anti-nerve growth factor receptor (NGFR) (1:200, ab271290, Abcam) and anti-Vimentin (1:1,000, ab8978, Abcam) antibodies, then incubated with corresponding secondary antibodies for 1 h at room temperature: goat anti-rabbit IgG (H+L) (1:500, 111-035-003, Jackson ImmunoResearch Laboratories, Inc.), donkey anti-mouse Alexa Fluor™ 488 (1:1,000, A-21202, Invitrogen; Thermo Fisher Scientific, Inc.), donkey anti-rabbit Alexa Fluor™ 555 (1:1,000, A-31572, Invitrogen; Thermo Fisher Scientific, Inc.) or goat anti-rat Alexa Fluor™ 647 (1:1,000, ab150159, Abcam). Images were captured using an Olympus VS200 slide scanner and Leica Thunder DMi8 Imager (Leica GmbH; magnification, x40).

For cryosectioning (15 μm), fixed tissues were dehydrated in 20 and 30% sucrose solution before embedding in the optimal cutting temperature compound (Sakura Finetek). Immunofluorescence staining was performed following standard protocols. The sections were blocked with QuickBlock™ Blocking Buffer (Beyotime Institute of Biotechnology) for 30 min at room temperature and incubated with antibodies against GSDMD (1:400, AF4012, Affinity Biosciences), SOX9 (1:400, ab185966, Abcam), SOX2 (1:200, 14-9811-82, Invitrogen; Thermo Fisher Scientific, Inc.), mucin 5 subtype AC (MUC5AC) (1:100, abs126767, Absin (Shanghai) Biotechnology Co., Ltd.), MUC5B (1:200, ab77995, Abcam), E-Cadherin (1:200, 20874-1-AP, Proteintech Group, Inc.) and Vimentin (1:1,000, ab8978, Abcam) at 4˚C overnight, and then incubated with secondary antibodies for 1 h at room temperature: donkey anti-mouse Alexa Fluor™ 488 (1:1,000, A-21202, Invitrogen; Thermo Fisher Scientific, Inc.), donkey anti-rabbit Alexa Fluor™ 555 (1:1,000, A-31572, Invitrogen; Thermo Fisher Scientific, Inc.) or goat anti-rat Alexa Fluor™ 647 (1:1,000; cat. no. ab150159, Abcam). Nuclei were counterstained with DAPI (Beyotime Institute of Biotechnology) for 10 min at room temperature. All samples were covered with ProLong™ Gold antifade reagent (Invitrogen; Thermo Fisher Scientific, Inc.). Fluorescence images were captured using a Leica Thunder DMi8 Imager and Stellaris STED confocal microscope (Leica GmbH; magnification, x40).

Measurement of hydroxyproline (HYP) content in peripheral lung tissue. The concentration of HYP was measured using a HYP assay kit (cat. no. A030-2-1, Nanjing Jiancheng Bioengineering Institute) according to the manufacturer's protocol. Peripheral lung tissue (60-90 mg) collected from the left lobe was hydrolyzed, and the results were calculated as μg HYP per g wet lung weight.

Western blotting. Peripheral lung tissue from the left lobe was homogenized in cold RIPA buffer (Thermo Fisher Scientific, Inc.) supplemented with protease and phosphatase inhibitors. Protein concentrations were measured using a bicinchoninic acid protein concentration assay kit according to the instructions (Beyotime Institute of Biotechnology). Equal amounts of protein (40 μg/lane) were subjected to electrophoresis on 8-12% SDS-PAGE and electroblotted PVDF membranes (MilliporeSigma). The membranes were blocked in 5% defatted milk (Beyotime Institute of Biotechnology) for 1 h at room temperature and then incubated at 4˚C overnight with the following primary antibodies: Anti-NLRP3 (1:500, NBP2-12446, Novus Biologicals, LLC), anti-pro-Caspase-1 (1:1,000, 24232, Cell Signaling Technology, Inc.), anti-ASC (1:1,000, 67824, Cell Signaling Technology, Inc.), anti-Caspase-1 p20 (1:1,000, 22915-1-AP, Proteintech Group, Inc.), anti-GSDMD (1:1,000, AF4012, Affinity Biosciences), anti-SOX9 (1:1,000, 82630, Cell Signaling Technology, Inc.), anti-SOX2 (1:1,000, ab97959, Abcam), anti-E-Cadherin (1:1,000, 14472, Cell Signaling Technology, Inc.), anti-Vimentin (1:1,000, ab8978, Abcam), anti-Sonic

hedgehog (Shh) (1:500, TA500040, OriGene Technologies, Inc.), anti-Smoothened (Smo) (1:1,000, ab236465, Abcam), anti-glioma-associated oncogene homolog-1 (Gli1) (1:2,000, NB600-600, Novus Biologicals, LLC), anti-Wnt10a (1:1,000, ab106522, Abcam), anti-phospho-glycogen synthase kinase-3β (p-GSK-3β) (1:1,000, 9336, Cell Signaling Technology, Inc.), anti-GSK-3β (1:1,000, 9315, Cell Signaling Technology, Inc.), anti-β-catenin (1:1,000, 8480, Cell Signaling Technology, Inc.), anti-β-actin (1:2,000, 20536-1-AP, Proteintech Group, Inc.) and anti-GAPDH (1:2,000, 10494-1-AP, Proteintech Group, Inc.). After incubation with horseradish peroxidase-conjugated secondary antibodies (1:8,000, 111-035-003/115-035-003, Jackson ImmunoResearch Laboratories, Inc.) for 1 h at room temperature, the membranes were incubated with WesternBright Quantum (Advansta, Inc.) and protein expression was quantified using a ChemiDoc™ XRS+ system with Image Lab 4.0 software (Bio-Rad Laboratories, Inc.).

Statistical analysis. Data were analyzed using SPSS 18.0 software (SPSS, Inc.) and are presented as the mean ± standard error of the mean of 3-6 independent experimental repeats. Statistical analysis was performed using one-way ANOVA followed by Tukey's post hoc test. $P<0.05$ was considered to indicate a statistically significant difference.

Results

Pharmacological inhibition of NLRP3 inflammasome improves pulmonary function in silica-treated mice. To evaluate the effects of NLRP3 inflammasome on lung tissue remodeling in silica-exposed mice, pulmonary function was assessed by measuring lung compliance and resistance (Fig. 2A-C). Although there was no significant difference in static compliance, dynamic compliance or airway resistance on day 7, the silica-treated group had worse pulmonary function than the other groups on days 28 and 56. MCC950-alone exerted little effect on pulmonary function, while it rescued the significant decrease in lung compliance and increase in airway resistance induced by silica at day 56. These results demonstrated that inhibiting NLRP3 inflammasome activation improved pulmonary function in silica-treated mice.

Inhibition of NLRP3 inflammasome alleviates distal lung remodeling by inhibiting the fibrotic response in silica-treated mice. The role of the NLRP3 inflammasome in the silica-induced fibrotic response in distal lung was further evaluated. Masson's trichrome staining indicated that silica induced excess collagen hyperplasia in the terminal bronchiole (Fig. 3A) and alveolar region (Fig. 3B). In addition, intratracheal instillation of silica suspension triggered a significant pulmonary fibrotic response (increases in positive Masson's trichrome staining and fibrosis score) in the distal lung starting on day 28 (Fig. 3A-C). Collagen deposition measured by hydroxyproline assay revealed that although MCC950-alone had no significant effect, it alleviated the lung fibrotic response in silica-treated mice, especially during chronic fibrosis (day 56; Fig. 3D).

Inhibition of NLRP3 inflammasome ameliorates distal lung inflammatory response in silica-treated mice. Effects of

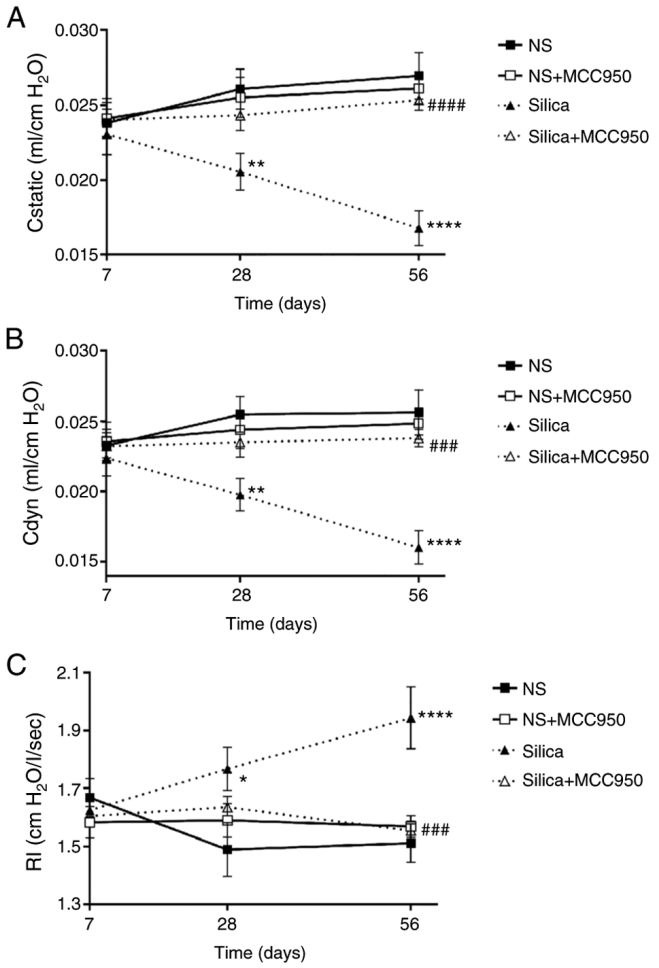

Figure 2. Pulmonary function evaluation of silica-treated mice. (A) Cstatic. (B) Cdyn. (C) Airway resistance. $^{*}P<0.05$, $^{**}P<0.01$, $^{****}P<0.0001$ vs. NS; $^{###}P<0.001$, $^{####}P<0.0001$ vs. silica. Cstatic, static compliance; Cdyn, dynamic compliance; RI, airway resistance index; NS, normal saline.

inhibition of the NLRP3 inflammasome on the silica-induced inflammatory response in the distal lung were investigated. H&E staining confirmed that intratracheal instillation of silica suspension induced diffuse infiltration of inflammatory cells in the terminal bronchiole (Fig. S1A) and alveolar region (Fig. S1B), which was consistent with increases in inflammation score on days 7, 28 and 56 (Fig. 4A). Moreover, inflammatory cell count, including neutrophils, lymphocytes and monocytes in BALF (Fig. 4B) and the concentrations of pro-inflammatory cytokines (IL-1β, IL-18 and TNF-α) and anti-inflammatory factor (IL-10) in BALF (Fig. 4C) revealed that MCC950 ameliorated lung inflammatory responses in silica-treated mice, especially during acute inflammation (day 7).

Instillation of a silica suspension leads to sustained NLRP3 inflammasome activation and pyroptosis in the distal lung. As silica is a well-recognized activator of the NLRP3 inflammasome (35,36), NLRP3 inflammasome activation was investigated. Both western blot (Fig. 5A-D) and immunohistochemical (Figs. S2A-C and S3A-C) analysis of components and products of the NLRP3 inflammasome (including NLRP3, pro-Caspase-1, ASC, Caspase-1 p20 and IL-1β) confirmed that

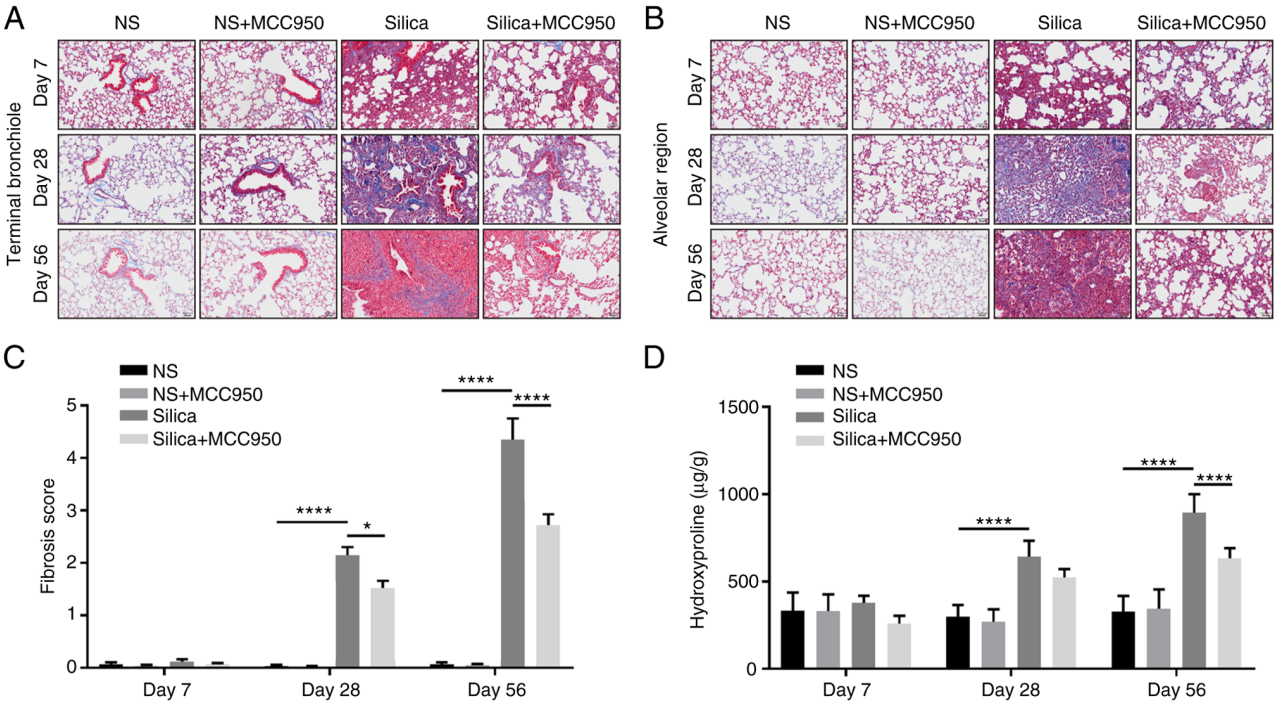

Figure 3. Distal lung fibrosis in silica-treated mice. Representative photographs of Masson's trichrome staining in (A) terminal bronchiole and (B) alveolar region. Scale bar, 50 μm. (C) Effects of MCC950 on silica exposure-induced fibrosis score in distal lung tissue. (D) Measurement of collagen deposition in peripheral lung tissue by hydroxyproline assay (n=6). *P<0.05, ****P<0.0001. NS, normal saline.

single intratracheal instillation of silica suspension resulted in sustained activation of the NLRP3 inflammasome, which was significantly suppressed by pharmacological inhibition of the NLRP3 inflammasome using MCC950. In addition, representative immunohistochemical staining of the terminal bronchiole (Fig. S2A-C) and alveolar region (Fig. S3A-C) indicated sustained NLRP3 inflammasome activation in the development of silica-induced progressive epithelial remodeling of the distal lung.

NLRP3-dependent pyroptosis is an autolytic programmed cell death characterized by membrane rupture and release of proinflammatory intracellular contents (36). Once activated, NLRP3 inflammasome downstream of Caspase-1 cleaves cytoplasmic GSDMD to release an active N-terminal domain to induce pyroptotic cell death (37). Western blotting revealed that, compared with the control, single silica instillation persistently upregulated expression of GSDMD N-terminal, which was reversed by the NLRP3 inflammasome inhibitor MCC950 (Fig. 6A). Similarly, immunofluorescence analysis showed that silica caused more membrane-distributed GSDMD^{+} cells (evidence of pyroptosis activation) (38) in the terminal bronchiole, which was alleviated by MCC950 (Fig. 6B). Furthermore, pyroptotic cells were mainly epithelial cells, including club cells (CC10^{+}) and ectopic basal cells (NGFR^{+}) (Fig. S4).

Silica-induced sustained NLRP3 inflammasome activation enhances cell proliferation, mucus production and epithelial-mesenchymal transition (EMT) in the distal lung. The effects of silica-induced NLRP3 inflammasome activation on cell proliferation, mucus production and EMT in the distal lung were further investigated. Immunofluorescence revealed that single administration of silica suspension led to progressively increased cell proliferation and mucus (MUC5AC/MUC5B) production in the terminal bronchiole, which were significantly suppressed by NLRP3 inflammasome inhibitor MCC950 (Fig. 7A and B). Moreover, proliferative cells were fibroblasts (Vimentin^{+}; key effector cells in the pathogenesis of pulmonary fibrosis (39); Fig. S5). Additionally, silica exposure promoted EMT of cells in the distal lung during the development of pulmonary fibrosis, with decreased E-Cadherin (epithelial marker) and increased Vimentin (mesenchymal marker) (40), especially in the chronic fibrotic phase (day 56; Fig. 7C). Western blotting demonstrated consistent results with the immunofluorescence assays (Fig. 7D and E). MCC950-alone did not affect the expression of EMT-associated markers in control mice, but reversed the silica-induced downregulation of E-Cadherin and upregulation of Vimentin on days 28 and 56 (Fig. 7D and E).

Silica-induced NLRP3 inflammasome activation causes abnormal repair and regeneration in the distal lung. Based on the findings that inhibition of the NLRP3 inflammasome alleviated epithelial remodeling in the distal lung, the reparative and regenerative behaviors of cells in this region in response to silica challenge were investigated. SOX9 and SOX2 are important factors related to lung repair and regeneration (41,42), and SOX9^{+}SOX2^{+} progenitor cells play a major role in embryonic lung branching morphogenesis by specifying proximal-distal fate (43). In terminal bronchiole, SOX9/SOX2 double-positive cells were not detected in the control or MCC950-only group but were abundant in the silica-treated group on day 7 (Fig. 8A). However, MCC950 significantly suppressed the expression of these double-positive cells. Consistently, western

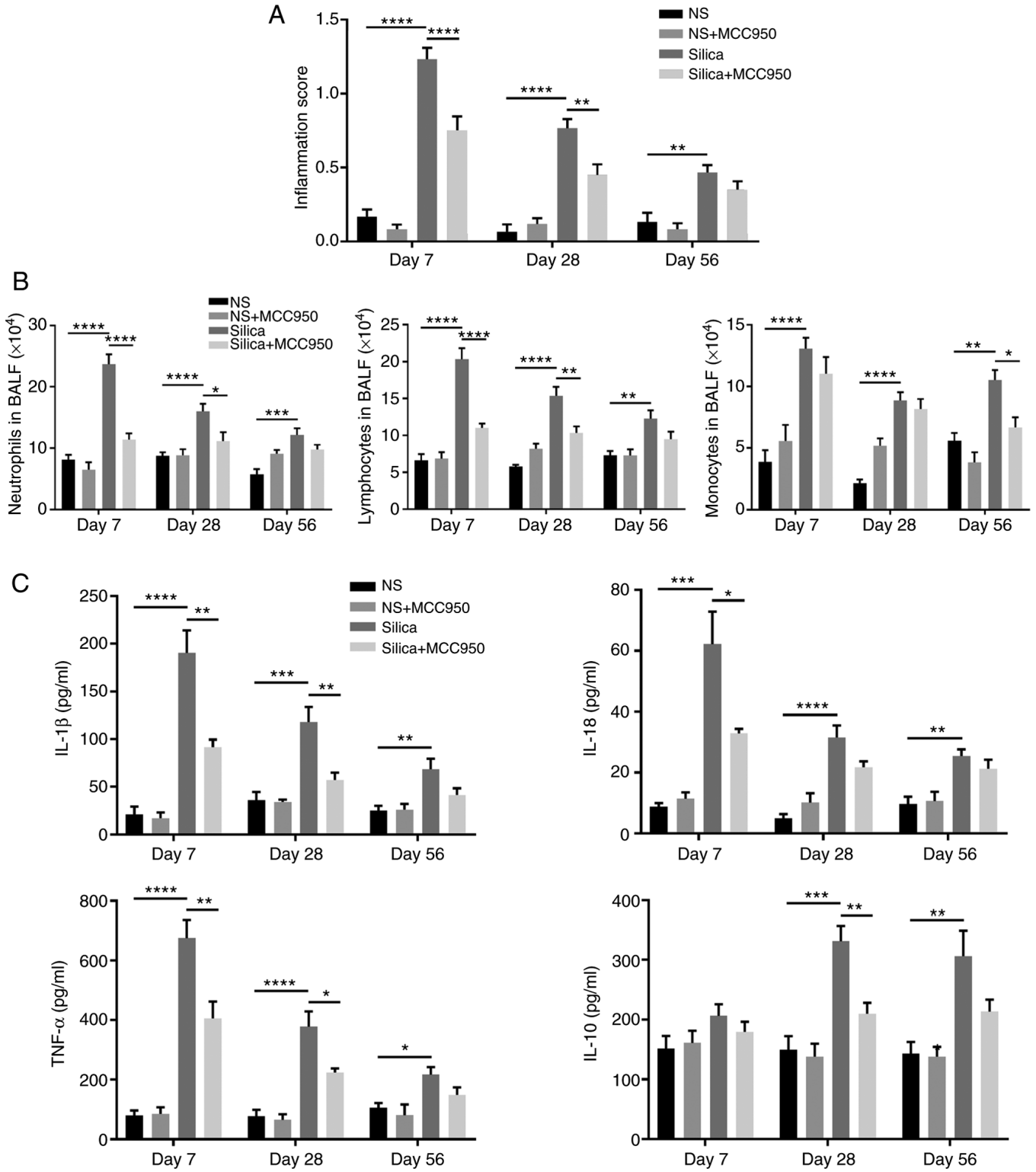

Figure 4. Evaluation of distal lung inflammation in silica-treated mice. (A) Effects of MCC950 on silica exposure-induced inflammation score in distal lung tissue. (B) Analysis of cell populations in the BALF of mice at 7, 28 and 56 days (n=6). (C) Measurement of cytokine levels in the BALF of mice at 7, 28 and 56 days (n=4-5). *P<0.05, **P<0.01, ***P<0.001, ****P<0.0001. BALF, bronchoalveolar lavage fluid; NS, normal saline.

blotting showed that silica instillation markedly upregulated levels of SOX9 and SOX2 on day 7, which were decreased by MCC950 (Fig. 8B and C). Non-significant alterations in SOX9 and SOX2 were observed between the four groups on days 28 and 56. Dual fluorescence staining assay using club cell-specific antibody CC10 and type II alveolar epithelial cell biomarker SPC to identify BASCs. Although few co-stained cells were detected at the BADJ (Fig. 8D), these BASCs were distributed in the alveolar region on day 7 (Fig. 8E). These ectopic BASCs were not observed following MCC950 treatment, leaving only SPC-positive type II alveolar epithelial cells (Fig. 8E). Taken together, these data demonstrated that

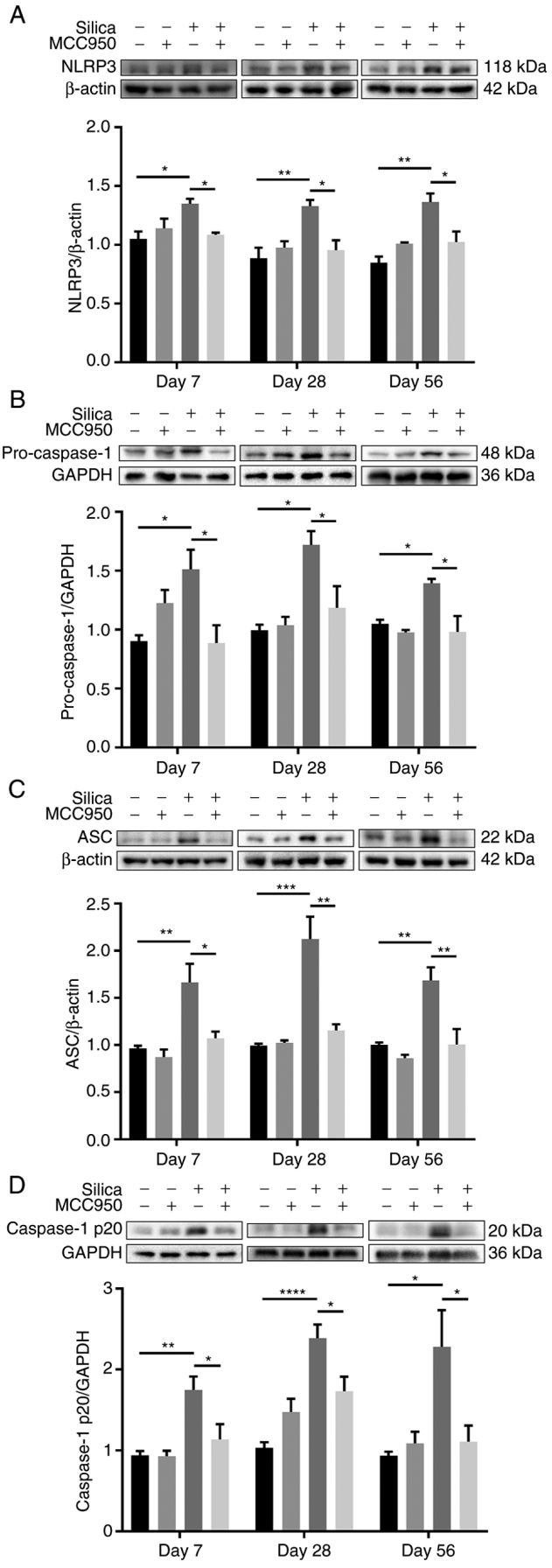

Figure 5. NLRP3 inflammasome activation. Representative western blotting of (A) NLRP3, (B) pro-Caspase-1, (C) ASC and (D) Caspase-1 p20 in peripheral lung tissues (n=3-5). *P<0.05, **P<0.01, ***P<0.001, ****P<0.0001. ASC, apoptosis-associated speck-like protein containing a CARD domain.

the NLRP3 inflammasome mediated silica-induced dysregulated repair and regeneration in the distal lung on day 7 after initial exposure, which were restored by MCC950 treatment.

Shh/Gli and Wnt/β-catenin pathways are involved in NLRP3 inflammasome-mediated epithelial remodeling and dysregulated regeneration in the distal lung. Previous studies have demonstrated that aberrant activation of the hedgehog signaling pathway, which serves a crucial role in lung homeostasis and tissue injury repair, is linked to pulmonary fibrosis (44,45). Compared with the control, silica administration significantly increased the expression of Shh, a major ligand of the hedgehog pathway (46), along with its downstream transmembrane protein Smo and responsive transcription factor Gli1 at all time points (Fig. 9A). However, following treatment with MCC950, the upregulation was effectively rescued compared with that in mice treated only with silica (Fig. 9A). Wnt pathway is key for lung homeostasis and tissue repair after injury (47,48). Wnt10a, a member of the Wnt family and key factor in pulmonary fibrosis (49), was markedly upregulated in the peripheral lung of silica-treated mice (Fig. 9B). Consistently, silica induced increases in the levels of Wnt downstream signaling proteins, including p-GSK-3β and β-catenin, both of which were significantly downregulated by NLRP3 inflammasome inhibitor MCC950 (Fig. 9C).

Discussion

Long-term inhalation and retention of crystalline silica particles leads to silicosis, an irreversible occupational pulmonary disease characterized by pulmonary fibrosis and silicon nodule formation (50). Currently, available management strategies are focused on control of associated symptoms (including chest tightness and dyspnea) and complications (including respiratory failure and lung cancer); there is no effective treatment for silicosis. Silica is a strong activator of the NLRP3 inflammasome (35,36) and enhances the inflammatory microenvironment by release of IL-1β and IL-18, as well as pyroptosis with cell swelling and rupture, which further promote NLRP3 activation and tissue damage (37). Moreover, recent preclinical findings in mouse models of pulmonary fibrosis confirmed a key role for the NLRP3 inflammasome in silica-driven chronic inflammation and irreversible fibrosis (28,51). Once inhaled, respirable silica particles permeate the lung to reach distal bronchioles and alveoli and are difficult to remove or degrade due to their physicochemical properties (crystals; small particles), initiating a cycle of persistent inflammation and repetitive injury. Silica-induced NLRP3 inflammasome activation leads to excessive release of inflammatory cytokines such as IL-1β, enhancing the inflammatory microenvironment surrounding deposited silica crystals and inducing inflammatory responses, including neutrophil infiltration and increased production of cytokines such as TNF-α (28,35). Moreover, when stimulated by these inflammatory cytokines, epithelial cells lose canonical features and acquire a mesenchymal phenotype, known as EMT, leading to excessive deposition of extracellular matrix (52). Therefore, the NLRP3 inflammasome represents a promising therapeutic target for silica-associated lung injuries and diseases.

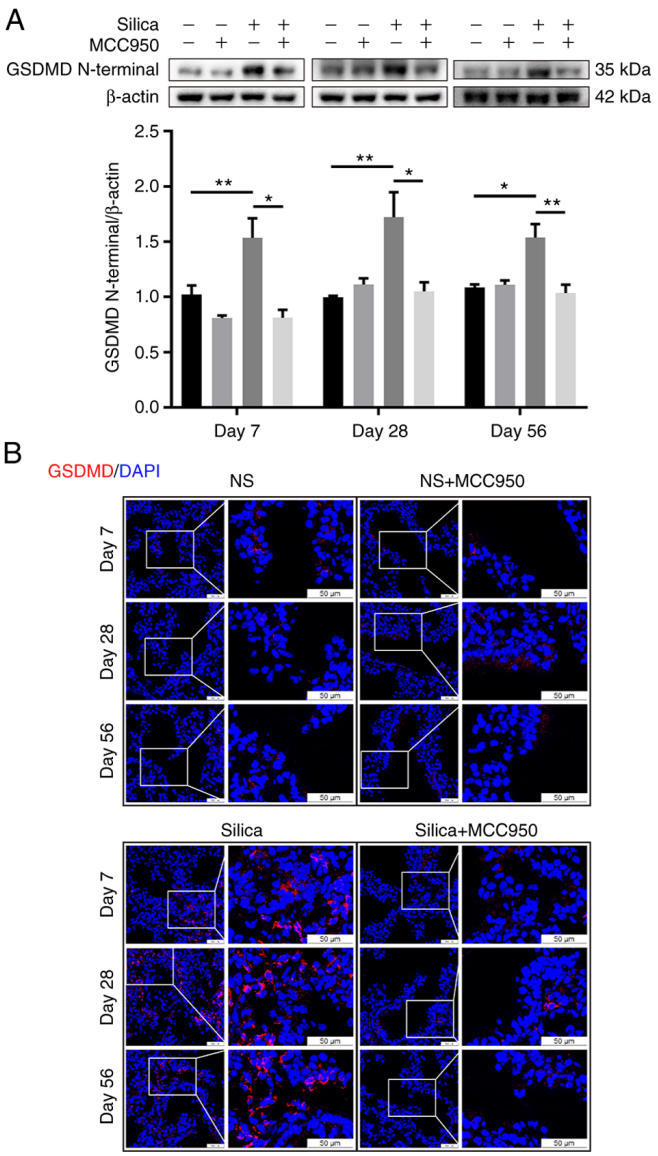

Figure 6. Effect of silica-induced NLRP3 inflammasome activation on pyroptosis in the distal lung. (A) Representative western blotting of GSDMD N-terminal domains (n=3-4). (B) Representative images of immunofluorescence staining for active GSDMD (red) in the terminal bronchiole. Scale bar, 50 μm. *P<0.05, **P<0.01. GSDMD, gasdermin D; NS, normal saline.

Although sufficient evidence indicates that the NLRP3 inflammasome serves an essential role in silica-induced lung inflammation and fibrosis (28,29,51,53), its effects on distal lung remodeling, repair and regeneration in different phases are poorly understood. The lung exhibits low levels of cell regeneration during normal homeostasis but displays a notable capacity for repair and regeneration following injury (54,55). However, dysfunctional or dysregulated epithelial repair in the distal lung contributes to tissue remodeling and fibrosis in chronic lung disease, such as COPD and idiopathic pulmonary fibrosis (IPF) (14,56,57). In particular, the distal lung is susceptible to silica-induced injury due to deposition in the terminal regions of the lung (5). In the initial inflammatory microenvironment, resident stem cells in the distal lung are recruited to repair damaged tissue. Once damage is eliminated, the acute inflammatory reaction subsides, allowing the restoration of tissue structure and functional recovery (58,59). Here, by using a long-term mouse model of silicosis, the role of the NLRP3 inflammasome in triggering pulmonary inflammation and fibrosis and its contribution to epithelial remodeling and dysregulated regeneration in the distal lung during different periods was investigated. Days 7, 28 and 56 were defined as the early, middle and late phases of silicosis, respectively. The early phase is dominated by the inflammatory response, while the final phase is dominated by the fibrotic response; chronic inflammation initiates fibrosis (60). In addition, increased mucin production occurs in response to persistent silica stimulation in fibrotic development, which presents a challenge for the function of the local stem/progenitor cells. Here, there was an increase in SOX9 and SOX2 in the terminal bronchiole only on day 7, as well as an ectopic distribution of BASCs in the alveolar region, which may be reparative responses to rebuild functional respiratory units in the early stage of silica-induced pulmonary fibrosis (61,62).

Under physiological conditions, pulmonary defense and function are dependent on normal mucus production and clearance (63). However, increased mucus production in the distal lung is observed in response to constant silica stimulation, which is one of the primary causes of airway blockage and increased resistance (64). Previous studies have reported that excessive mucus accumulation in the distal lung leads to recurrent injury/inflammation/repair cycles with defective mucociliary clearance and mucosal host defense (65-67). Here, silica-induced sustained NLRP3 inflammasome activation resulted in MUC5AC or MUC5B overproduction as a repair response to distal lung injuries during silica-induced chronic pulmonary inflammation and fibrosis. MUC5AC and MUC5B are the primary glycoprotein components of airway mucus that are involved in local defense of the airway and lung homeostasis (68) but their overexpression is a feature of inflammatory airway diseases and is associated with adverse pulmonary outcomes (69). Specifically, MUC5AC is a secreted gel-forming mucin produced by superficial airway goblet cells; excessive MUC5AC production serves a detrimental role in lung inflammation and injury (69,70), as well as airway diseases such as COPD and cystic fibrosis (CF) (71). By contrast, MUC5B is predominantly expressed in submucosal glands and is key for homeostatic defense (71). However, excessive MUC5B aggregation impairs mucosal host defense and results in excessive lung injury from inhaled substances (70). For example, accumulation of MUC5B initiates the muco-obstructive process in CF, leads to development of idiopathic interstitial pneumonia and causes mucociliary dysfunction and enhanced lung fibrosis in mouse models (70,72,73). The present study showed that targeted suppression of mucin hypersecretion by the NLRP3 inflammasome during the development of pulmonary fibrosis improved epithelial remodeling and pulmonary fibrosis, which may be implicated in the functional conservation of local stem/progenitor cells in the distal lung upon silica challenge. This is consistent with our previous observations in a mouse lung stem/progenitor cell-derived organotypic model (40).

In mouse lung development, proximal-distal patterning is defined by two key transcription factors, SOX2 and SOX9, which are exclusively localized in the proximal and distal epithelium, respectively (74,75). The specific distribution promotes proper branching morphogenesis, including proximal

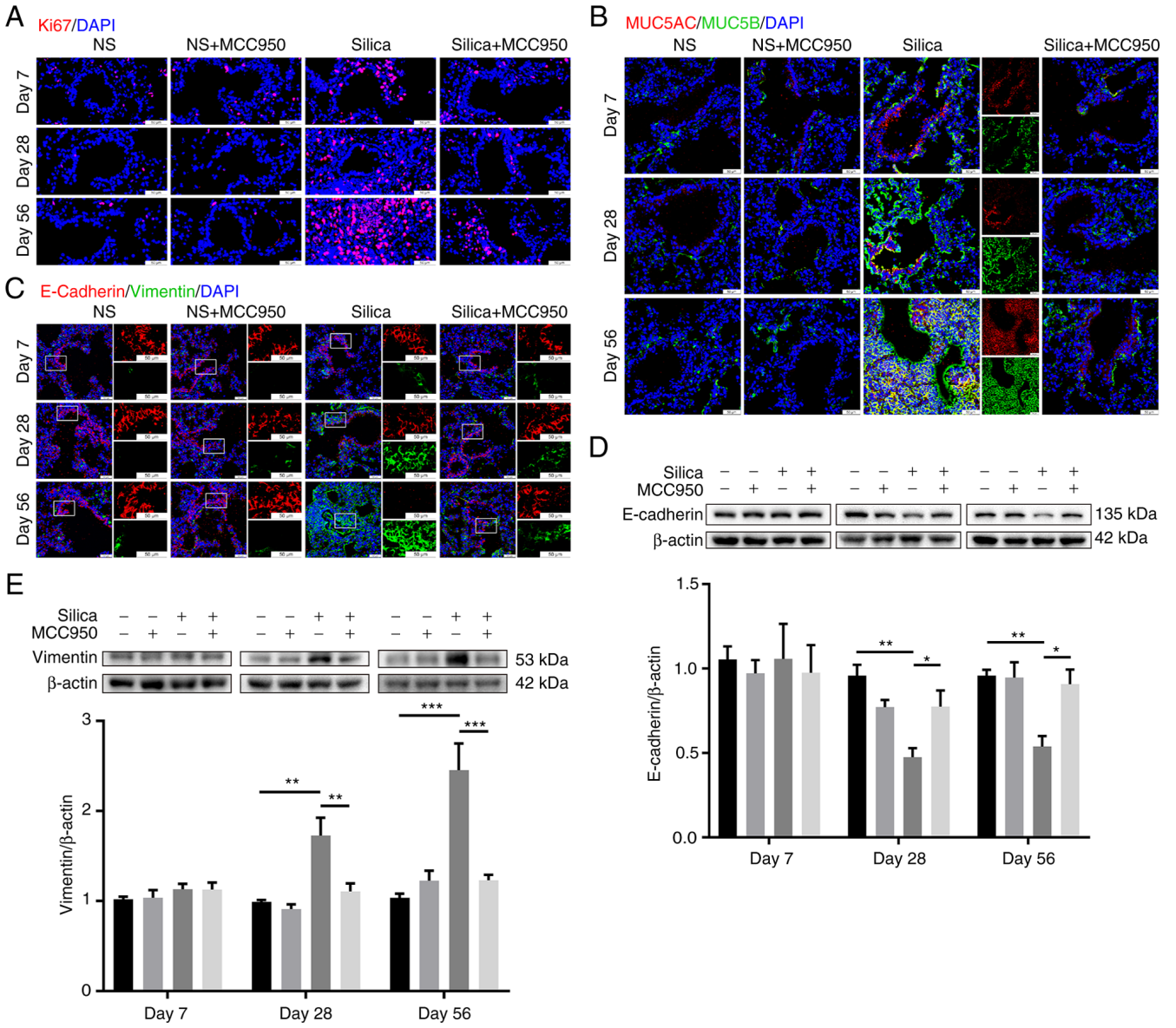

Figure 7. Effect of silica-induced NLRP3 inflammasome activation on cell proliferation, mucus production and epithelial-mesenchymal transition. Representative immunostaining of (A) Ki67 (red; scale bar, 20 μm), (B) MUC5AC (red) and MUC5B (green) and (C) E-Cadherin (red) and Vimentin (green) in the terminal bronchiole. Scale bar, 50 μm. Representative western blotting of (D) E-Cadherin and (E) Vimentin (n=3-4). *P<0.05, **P<0.01, ***P<0.001. MUC5AC, mucin 5 subtype AC; NS, normal saline.

air-conducting airways and distal gas-exchanging alveoli. Prior to this, when maximal branching occurs, a progenitor cell population co-expressing SOX2 and SOX9 is present in the distal tips of the branching epithelium, which is lost as branching proceeds (74). Furthermore, although the population exhibits an enhanced proliferative potential in developing lungs, such potential is rare in adult distal lungs (74,76). Here, after silica exposure for 7 days, the SOX9/SOX2 double-positive population reappeared in the terminal bronchiole, with a concurrent increase in levels of SOX9 and SOX2 in the peripheral lungs. Additionally, SOX9/SOX2 double-positive cells in the distal lung were lost on days 28 and 56 and no significant differences in SOX9 and SOX2 levels were observed. Our previous study demonstrated that the proportion of $SOX9^{+}SOX2^{+}$ cells is increased in silica-treated air-liquid interface cultures, which contributes to hyperproliferation and abnormal differentiation of the lung stem/progenitor cell-derived airway epithelium (40). Furthermore, BADJ is a novel regenerative microenvironment that has a population of rare stem cells called BASCs that can self-renew over multiple passages and contribute to maintenance of both bronchiolar and alveolar lineages (17,18,77). Similar to the aberrant spatiotemporal expression of SOX2 and SOX9, the silica-induced NLRP3 inflammasome disrupted distribution of BASCs, which were ectopically expressed in the alveolar region on day 7 after silica exposure. By contrast, BASCs were almost undetectable in the alveolar areas of silica-exposed mice on days 28 and 56 and were rare at the BADJ in all groups at all time points. The regenerative potential of stem/progenitor cells relies on correct spatial localization and temporal expression (78-80) and these specific cell populations appearing only in the early inflammatory phase represent a hyperproliferative state to repair the distal lung epithelium in response to silica stimulation. However, sustained silica stimulation led to persistent activation of the NLRP3 inflammasome and caused

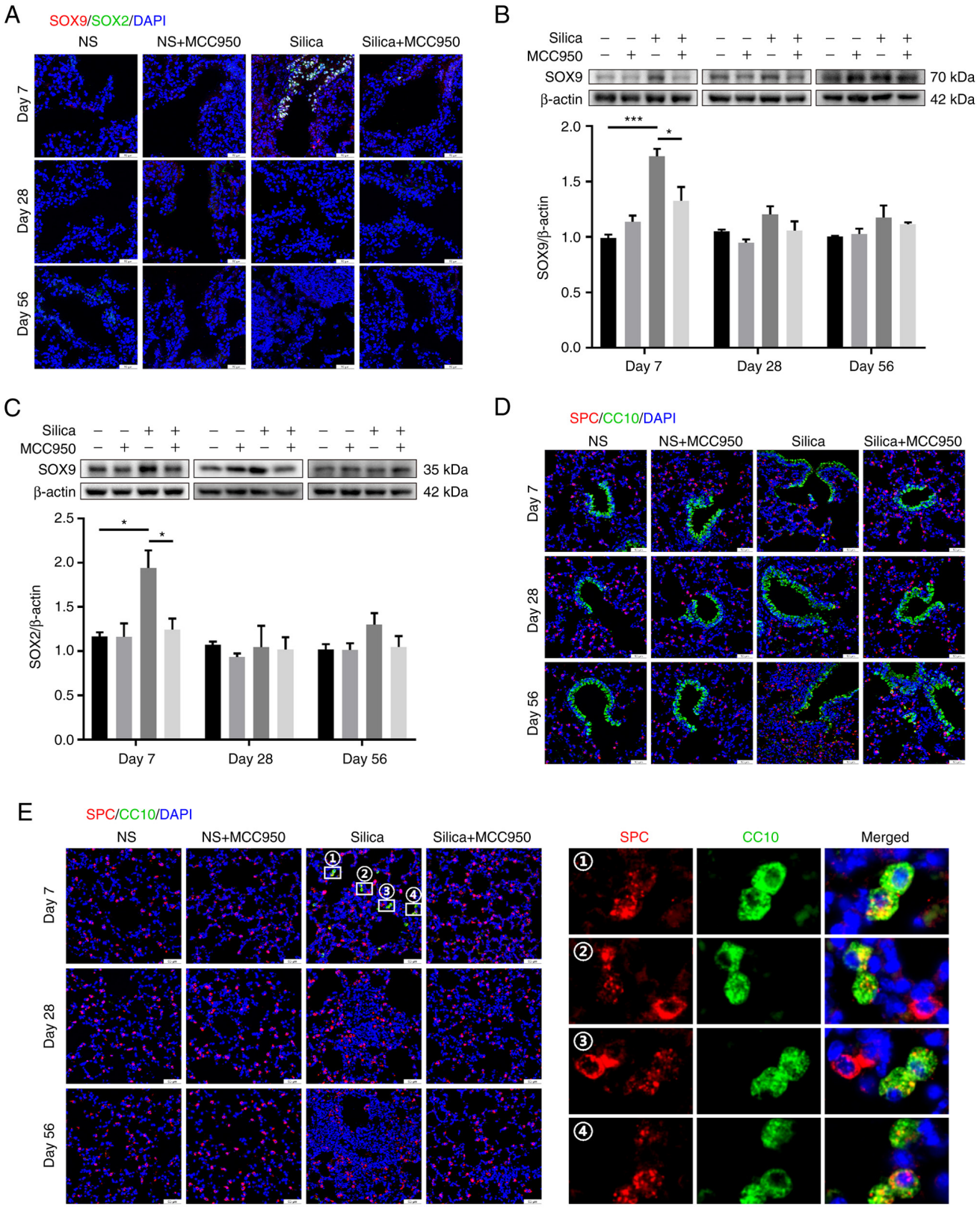

Figure 8. Effects of silica-induced NLRP3 inflammasome activation on aberrant reparative and regenerative behaviors of cells in the distal lung. (A) Representative immunofluorescence staining for SOX9 (red) and SOX2 (green) in the terminal bronchiole. Representative western blotting of (B) SOX9 and (C) SOX2 in peripheral lung tissue (n=3-4). Representative immunofluorescence staining for SPC (red) and CC10 (green) at the (D) BADJ and (E) in the alveolar region. Scale bar, 50 μm. *P<0.05, ***P<0.001. SPC, surfactant protein C; CC10, club cell 10 kDa protein; BADJ, bronchoalveolar duct junction; NS, normal saline.

continuous inflammatory responses, ultimately destroying inflammatory homeostasis and leading to depletion of stem cells that promoted epithelial remodeling and pulmonary fibrosis. However, these abnormalities on day 7 were effectively

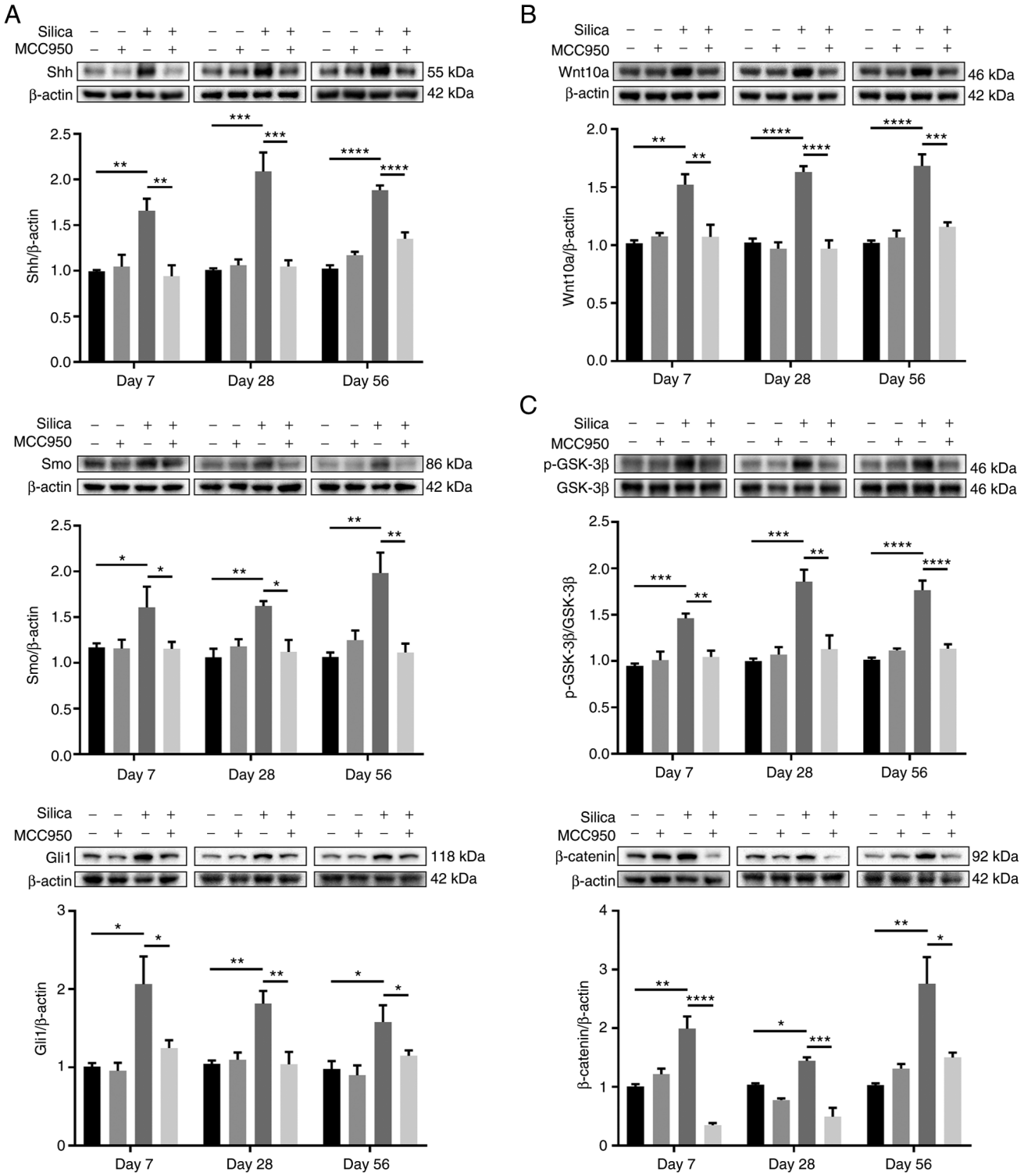

Figure 9. Effect of silica-induced NLRP3 inflammasome activation on the Shh/Gli and Wnt/β-catenin pathways in the peripheral lung. Western blotting of (A) Shh/Gli pathway-related proteins Shh (n=4), Smo (n=3-4) and Gli1 (n=4), (B) Wnt10a (n=4) and (C) canonical Wnt/β-catenin pathway-related molecules p-GSK-3β (n=4) and β-catenin (n=3). *P<0.05, **P<0.01, ***P<0.001, ****P<0.0001. Shh, Sonic hedgehog; Gli, glioma-associated oncogene; Smo, Smoothened; p-GSK-3β, phospho-glycogen synthase kinase-3β.

ameliorated by NLRP3 inflammasome inhibition, indicating that NLRP3 inflammasome activation may be a central event in dysregulated regeneration in the distal lung during the early inflammatory phase of silica-induced epithelial remodeling. Although the role of the NLRP3 inflammasome in spatiotemporal regulation of these cell populations is unclear, the initial inflammatory microenvironment induced by the activated NLRP3 inflammasome may alter development-associated signals to modulate repair and regeneration of the distal lung.

Increasing evidence indicates that aberrant activation of lung developmental signals, including the Shh/Gli and Wnt/β-catenin pathways, is associated with fibrotic lung

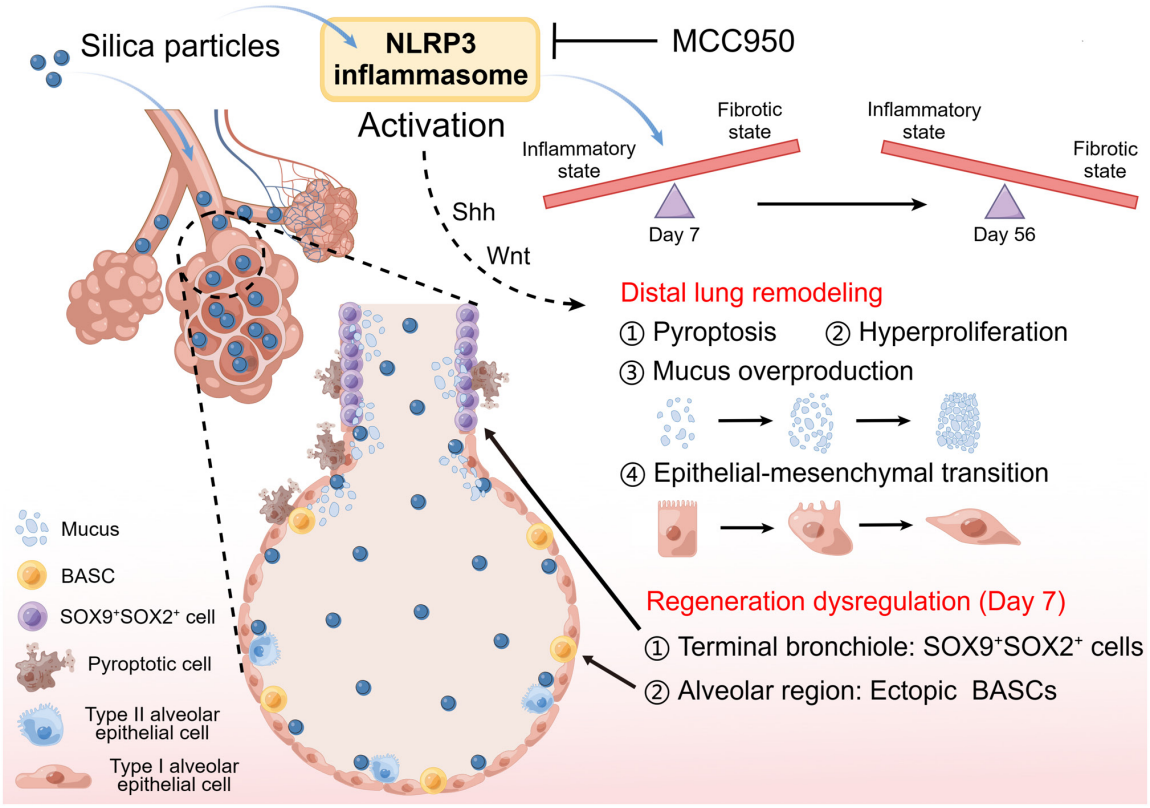

Figure 10. Graphical summary. Effects of the NLRP3 inflammasome on abnormal epithelial regeneration and distal lung remodeling in silica-induced lung fibrosis. Sustained activation of the NLRP3 inflammasome resulted in persistent inflammatory reactions, causing distal lung remodeling and regeneration dysregulation. Shh, Sonic hedgehog; BASC, bronchioalveolar stem cell. The graphical abstract was created by Figdraw (www.figdraw.com).

disease (49,75,81). It has been suggested that Shh/Gli signaling is significant not only in embryonic lung development and branching morphogenesis but also in repair and regeneration following injury to adult lungs (82,83). Although the Shh pathway is maintained at low levels after birth, it is reactivated in the lung epithelium in response to acute injury, signaling nearby cells and promoting stem cell proliferation and tissue repair to reestablish homeostasis and structural integrity (84). Once this is achieved, Shh levels return to normal. However, in the development of chronic lung inflammatory disease, higher expression of Shh is maintained, which signals inflammatory cell populations and supports sustained inflammatory responses, leading to tissue remodeling and regeneration failure (83,85,86). Similarly, Wnt/β-catenin signaling serves critical roles in the pathogenesis of chronic lung diseases, including lung fibrosis, and in repair and regeneration of the lung (47,87). Following acute lung injury, active canonical Wnt signaling is key for the proliferation and differentiation of lung epithelial stem/progenitor cells (47,81). However, in the fibrotic environment, chronic Wnt/β-catenin signaling activity induces senescence in lung epithelial cells, contributing to the dysfunction and reduction of progenitor cells, as well as impaired lung repair (88). Moreover, in IPF, continuous injury of lung epithelium promotes prolonged and chronic Wnt/β-catenin activity and further stimulates tissue remodeling and destruction (13,88). Furthermore, Wnt10a is an upstream activator of β-catenin in the canonical Wnt/β-catenin signaling pathway and its overexpression in lung-resident mesenchymal stem cells is associated with Shh/Gli activation (49), indicating signaling crosstalk between the Shh/Gli and Wnt/β-catenin pathways. In the present silica-induced mouse lung fibrosis model, key signaling molecules of the Shh and Wnt pathways were significantly upregulated at all time points and were effectively suppressed following treatment with MCC950. These results suggested that in addition to mediating inflammation and fibrosis, NLRP3 inflammasome activation also participated in the regulation of development- and regeneration-associated pathways. Although increased activity of these signals serves a functional role in guiding repair during acute inflammation and damage, their continuous upregulation signals to inflammatory cells promote epithelial remodeling and dysregulated regeneration. As the restoration or destruction of tissue structure is dependent on the duration of signal transduction, precise temporal regulation of NLRP3 inflammasome assembly may serve a protective role in lung repair and regeneration following injuries.

Taken together, the present data demonstrated that the NLRP3 inflammasome served a crucial role in silica-induced epithelial remodeling and dysregulated regeneration in a time-dependent manner in the distal lung of mice (Fig. 10). NLRP3 inflammasome activation in the early inflammatory phase promotes the migration and recruitment of stem/progenitor cells to promote tissue repair and functional recovery but its sustained activation results in persistent inflammatory reactions, causing depletion of stem/progenitor cells, subsequent regeneration failure and epithelial remodeling (40). Therefore, detection of the early stage of inhalable particle-related lung disease and precise control of NLRP3 inflammasome

activation to enhance normal epithelial repair and regeneration are of clinical importance to avoid irreversible damage.

Acknowledgements

Not applicable.

Funding

The present study was supported by National Key Research & Development Program of China (grant no. 2022YFF0710800), National Natural Science Foundation of China (grant no. 81870054) and the Key Project of National Science & Technology for Infectious Diseases of China (grant no. 2018ZX10722301).

Availability of data and materials

The data generated in the present study may be requested from the corresponding author.

Authors' contributions

HZ, QZ and HK designed the study. HZ, CL and JF performed the experiments and analyzed data. HZ wrote the manuscript. WH, NL and MY collected and interpreted data and provided technological assistance. HW, WX and HK analyzed and interpreted data. HZ and HK revised the manuscript and confirm the authenticity of all the raw data. All authors have read and approved the final manuscript.

Ethics approval and consent to participate

All experimental procedures involving mice were approved by the Institutional Animal Care and Use Committee of Nanjing Medical University (approval no. NJMU/IACUC-2012034).

Patient consent for publication

Not applicable.

Competing interests

The authors declare that they have no competing interests.

References

1. Christenson SA, Smith BM, Bafadhel M and Putcha N: Chronic obstructive pulmonary disease. Lancet 399: 2227-2242, 2022.
2. Aghapour M, Ubags ND, Bruder D, Hiemstra PS, Sidhaye V, Rezaee F and Heijink IH: Role of air pollutants in airway epithelial barrier dysfunction in asthma and COPD. Eur Respir Rev 31: 210112, 2022.
3. Takada T, Moriyama H and Suzuki E: Elemental analysis of occupational and environmental lung diseases by electron probe microanalyzer with wavelength dispersive spectrometer. Respir Investig 52: 5-13, 2014.
4. Leung CC, Yu IT and Chen W: Silicosis. Lancet 379: 2008-2018, 2012.
5. Ma J, Cai Q, Yang D, Yang J, Xue J, Yu M, Liu Y, Ma F, Li F and Liu X: A positive feed forward loop between Wnt/β-Catenin and NOX4 promotes silicon dioxide-induced epithelial-mesenchymal transition of lung epithelial cells. Oxid Med Cell Longev 2020: 3404168, 2020.
6. Koudstaal T, Funke-Chambour M, Kreuter M, Molyneaux PL and Wijsenbeek MS: Pulmonary fibrosis: From pathogenesis to clinical decision-making. Trends Mol Med 29: 1076-1087, 2023.
7. Aggarwal K, Arora S and Nagpal K: Pulmonary Fibrosis: Unveiling the pathogenesis, exploring therapeutic targets, and advancements in drug delivery strategies. AAPS PharmSciTech 24: 152, 2023.
8. Yu Q, Fu G, Lin H, Zhao Q, Liu Y, Zhou Y, Shi Y, Zhang L, Wang Z, Zhang Z, *et al*: Influence of silica particles on mucociliary structure and MUC5B expression in airways of C57BL/6 mice. Exp Lung Res 46: 217-225, 2020.
9. Li S, Li Y, Zhang Y, Li S, Zhang M, Jin F, Wei Z, Yang Y, Gao X, Mao N, *et al*: N-Acetyl-Seryl-Asparyl-Lysyl-Proline regulates lung renin angiotensin system to inhibit epithelial-mesenchymal transition in silicotic mice. Toxicol Appl Pharmacol 408: 115255, 2020.
10. Yang J, Wu S, Hu W, Yang D, Ma J, Cai Q, Xue J, Chen J, Li F, Zeng J and Liu X: Bmi1 signaling maintains the plasticity of airway epithelial progenitors in response to persistent silica exposures. Toxicology 470: 153152, 2022.
11. Churg A and Wright JL: Bronchiolitis caused by occupational and ambient atmospheric particles. Semin Respir Crit Care Med 24: 577-584, 2003.
12. Ferreira TP, de Arantes AC, do Nascimento CV, Olsen PC, Trentin PG, Rocco PR, Hogaboam CM, Puri RK, Martins MA and Silva PM: IL-13 immunotoxin accelerates resolution of lung pathological changes triggered by silica particles in mice. J Immunol 191: 5220-5229, 2013.
13. Crosby LM and Waters CM: Epithelial repair mechanisms in the lung. Am J Physiol Lung Cell Mol Physiol 298: L715-L731, 2010.
14. Ptasinski VA, Stegmayr J, Belvisi MG, Wagner DE and Murray LA: Targeting alveolar repair in idiopathic pulmonary fibrosis. Am J Respir Cell Mol Biol 65: 347-365, 2021.
15. Salahudeen AA, Choi SS, Rustagi A, Zhu J, van Unen V, de la O SM, Flynn RA, Margalef-Català M, Santos AJM, Ju J, *et al*: Progenitor identification and SARS-CoV-2 infection in human distal lung organoids. Nature 588: 670-675, 2020.
16. Alanis DM, Chang DR, Akiyama H, Krasnow MA and Chen J: Two nested developmental waves demarcate a compartment boundary in the mouse lung. Nature Commun 5: 3923, 2014.
17. Kawakita N, Toba H, Miyoshi K, Sakamoto S, Matsumoto D, Takashima M, Aoyama M, Inoue S, Morimoto M, Nishino T, *et al*: Bronchioalveolar stem cells derived from mouse-induced pluripotent stem cells promote airway epithelium regeneration. Stem Cell Res Ther 11: 430, 2020.
18. Jones-Freeman B and Starkey MR: Bronchioalveolar stem cells in lung repair, regeneration and disease. J Pathol 252: 219-226, 2020.
19. Eisenhauer P, Earle B, Loi R, Sueblinvong V, Goodwin M, Allen GB, Lundblad L, Mazan MR, Hoffman AM and Weiss DJ: Endogenous distal airway progenitor cells, lung mechanics, and disproportionate lobar growth following long-term postpneumonectomy in mice. Stem Cells 31: 1330-1339, 2013.
20. Caseley EA, Lara-Reyna S, Poulter JA, Topping J, Carter C, Nadat F, Spickett GP, Savic S and McDermott MF: An atypical autoinflammatory disease due to an LRR domain NLRP3 mutation enhancing binding to NEK7. J Clin Immunol 42: 158-170, 2022.
21. Swanson KV, Deng M and Ting JP: The NLRP3 inflammasome: Molecular activation and regulation to therapeutics. Nat Rev Immunol 19: 477-489, 2019.
22. Burdette BE, Esparza AN, Zhu H and Wang S: Gasdermin D in pyroptosis. Acta Pharm Sin B 11: 2768-2782, 2021.
23. Liang Q, Cai W, Zhao Y, Xu H, Tang H, Chen D, Qian F and Sun L: Lycorine ameliorates bleomycin-induced pulmonary fibrosis via inhibiting NLRP3 inflammasome activation and pyroptosis. Pharmacol Res 158: 104884, 2020.
24. Zheng R, Tao L, Jian H, Chang Y, Cheng Y, Feng Y and Zhang H: NLRP3 inflammasome activation and lung fibrosis caused by airborne fine particulate matter. Ecotoxicol Environ Saf 163: 612-619, 2018.
25. Lamkanfi M and Dixit VM: Inflammasomes and their roles in health and disease. Annu Rev Cell Dev Biol 28: 137-161, 2012.
26. Song M, Wang J, Sun Y, Pang J, Li X, Liu Y, Zhou Y, Yang P, Fan T, Liu Y, *et al*: Inhibition of gasdermin D-dependent pyroptosis attenuates the progression of silica-induced pulmonary inflammation and fibrosis. Acta Pharm Sin B 12: 1213-1224, 2022.

27. Tapia-Abellán A, Angosto-Bazarra D, Martínez-Banaclocha H, de Torre-Minguela C, Cerón-Carrasco JP, Pérez-Sánchez H, Arostegui JI and Pelegrin P: MCC950 closes the active conformation of NLRP3 to an inactive state. Nat Chem Biol 15: 560-564, 2019.
28. Lam M, Mansell A and Tate MD: Another One Fights the Dust: Targeting the NLRP3 inflammasome for the treatment of silicosis. Am J Respir Cell Mol Biol 66: 601-611, 2022.
29. Sayan M and Mossman BT: The NLRP3 inflammasome in pathogenic particle and fibre-associated lung inflammation and diseases. Part Fibre Toxicol 13: 51, 2016.
30. Clark JD, Gebhart GF, Gonder JC, Keeling ME and Kohn DF: Special Report: The 1996 Guide for the Care and Use of Laboratory Animals. ILAR J 38: 41-48, 1997.
31. Zou Z, Hu X, Luo T, Ming Z, Chen X, Xia L, Luo W, Li J, Xu N, Chen L, *et al*: Naturally-occurring spinosyn A and its derivatives function as argininosuccinate synthase activator and tumor inhibitor. Nat Commun 12: 2263, 2021.
32. Zhao S, Zhou L, Wang Q, Cao JH, Chen Y, Wang W, Zhu BD, Wei ZH, Li R, Li CY, *et al*: Elevated branched-chain amino acid promotes atherosclerosis progression by enhancing mitochondrial-to-nuclear H_2O_2-disulfide HMGB1 in macrophages. Redox Biol 62: 102696, 2023.
33. Szapiel SV, Elson NA, Fulmer JD, Hunninghake GW and Crystal RG: Bleomycin-induced interstitial pulmonary disease in the nude, athymic mouse. Am Rev Respir Dis 120: 893-899, 1979.
34. Hübner RH, Gitter W, El Mokhtari NE, Mathiak M, Both M, Bolte H, Freitag-Wolf S and Bewig B: Standardized quantification of pulmonary fibrosis in histological samples. Biotechniques 44: 507-511, 514-507, 2008.
35. Campden RI, Warren AL, Greene CJ, Chiriboga JA, Arnold CR, Aggarwal D, McKenna N, Sandall CF, MacDonald JA and Yates RM: Extracellular cathepsin Z signals through the α_5 integrin and augments NLRP3 inflammasome activation. J Biol Chem 298: 101459, 2022.
36. Yin H, Fang L, Wang L, Xia Y, Tian J, Ma L, Zhang J, Li N, Li W, Yao S and Zhang L: Acute silica exposure triggers pulmonary inflammation through macrophage pyroptosis: An experimental simulation. Front Immunol 13: 874459, 2022.
37. Shi J, Gao W and Shao F: Pyroptosis: Gasdermin-Mediated programmed necrotic cell death. Trends Biochem Sci 42: 245-254, 2017.
38. Zhou YP, Mei MJ, Wang XZ, Huang SN, Chen L, Zhang M, Li XY, Qin HB, Dong X, Cheng S, *et al*: A congenital CMV infection model for follow-up studies of neurodevelopmental disorders, neuroimaging abnormalities, and treatment. JCI Insight 7: e152551, 2022.
39. Liu Y, Zhang X, Wang J, Yang F, Luo W, Huang J, Chen M, Wang S, Li C, Zhang W and Chao J: ZC3H4 regulates infiltrating monocytes, attenuating pulmonary fibrosis through IL-10. Respir Res 23: 204, 2022.
40. Zhou H, Zhang Q, Huang W, Zhou S, Wang Y, Zeng X, Wang H, Xie W and Kong H: NLRP3 inflammasome mediates silica-induced lung epithelial injury and aberrant regeneration in lung Stem/Progenitor Cell-Derived organotypic models. Int J Biol Sci 19: 1875-1893, 2023.
41. Chen S, Li K, Zhong X, Wang G, Wang X, Cheng M, Chen J, Chen Z, Chen J, Zhang C, *et al*: Sox9-expressing cells promote regeneration after radiation-induced lung injury via the PI3K/AKT pathway. Stem Cell Res Ther 12: 381, 2021.
42. Eenjes E, Tibboel D, Wijnen RMH, Schnater JM and Rottier RJ: SOX2 and SOX21 in lung epithelial differentiation and repair. Int J Mol Sci 23: 13064, 2022.
43. Belgacemi R, Danopoulos S, Deutsch G, Glass I, Dormoy V, Bellusci S and Al Alam D: Hedgehog signaling pathway orchestrates human lung branching morphogenesis. Int J Mol Sci 23: 5265, 2022.
44. Zhang J, Liu H, Song C, Zhang J, Wang Y, Lv C and Song X: Astilbin ameliorates pulmonary fibrosis via blockade of Hedgehog signaling pathway. Pulm Pharmacol Ther 50: 19-27, 2018.
45. Wang C, Cassandras M and Peng T: The role of hedgehog signaling in adult lung regeneration and maintenance. J Dev Biol 7: 14, 2019.
46. Li L, Bao J, Wang H, Lei JH, Peng C, Zeng J, Hao W, Zhang X, Xu X, Yu C, *et al*: Upregulation of amplified in breast cancer 1 contributes to pancreatic ductal adenocarcinoma progression and vulnerability to blockage of hedgehog activation. Theranostics 11: 1672-1689, 2021.
47. Raslan AA and Yoon JK: WNT Signaling in lung repair and regeneration. Mol Cells 43: 774-783, 2020.
48. Skronska-Wasek W, Mutze K, Baarsma HA, Bracke KR, Alsafadi HN, Lehmann M, Costa R, Stornaiuolo M, Novellino E, Brusselle GG, *et al*: Reduced frizzled receptor 4 expression prevents WNT/β-Catenin-driven alveolar lung repair in chronic obstructive pulmonary disease. Am J Respir Crit Care Med 196: 172-185, 2017.
49. Cao H, Chen X, Hou J, Wang C, Xiang Z, Shen Y and Han X: The Shh/Gli signaling cascade regulates myofibroblastic activation of lung-resident mesenchymal stem cells via the modulation of Wnt10a expression during pulmonary fibrogenesis. Lab Invest 100: 363-377, 2020.
50. Jiang R, Han L, Gao Q and Chao J: ZC3H4 mediates silica-induced EndoMT via ER stress and autophagy. Environ Toxicol Pharmacol 84: 103605, 2021.
51. Song MY, Wang JX, Sun YL, Han ZF, Zhou YT, Liu Y, Fan TH, Li ZG, Qi XM, Luo Y, *et al*: Tetrandrine alleviates silicosis by inhibiting canonical and non-canonical NLRP3 inflammasome activation in lung macrophages. Acta Pharmacol Sin 43: 1274-1284, 2022.
52. Pang X, Shao L, Nie X, Yan H, Li C, Yeo AJ, Lavin MF, Xia Q, Shao H, Yu G, *et al*: Emodin attenuates silica-induced lung injury by inhibition of inflammation, apoptosis and epithelial-mesenchymal transition. Int Immunopharmacol 91: 107277, 2021.
53. Song Z, Wang L, Cao Y, Liu Z, Zhang M, Zhang Z, Jiang S, Fan R, Hao T, Yang R,*et al*: Isoandrographolide inhibits NLRP3 inflammasome activation and attenuates silicosis in mice. Int Immunopharmacol 105: 108539, 2022.
54. Wujak L, Schnieder J, Schaefer L and Wygrecka M: LRP1: A chameleon receptor of lung inflammation and repair. Matrix Biol 68-69: 366-381, 2018.
55. Beers MF and Morrisey EE: The three R's of lung health and disease: Repair, remodeling, and regeneration. J Clin Invest 121: 2065-2073, 2011.
56. Spella M, Lilis I and Stathopoulos GT: Shared epithelial pathways to lung repair and disease. Eur Respir Rev 26: 170048, 2017.
57. Brandsma CA, de Vries M, Costa R, Woldhuis RR, Königshoff M and Timens W: Lung ageing and COPD: Is there a role for ageing in abnormal tissue repair? Eur Respir Rev 26: 170073, 2017.
58. Nakao M, Kim K, Nagase K, Grainger DW, Kanazawa H and Okano T: Phenotypic traits of mesenchymal stem cell sheets fabricated by temperature-responsive cell culture plate: Structural characteristics of MSC sheets. Stem Cell Res Ther 10: 353, 2019.
59. Hegdekar N, Sarkar C, Bustos S, Ritzel RM, Hanscom M, Ravishankar P, Philkana D, Wu J, Loane DJ and Lipinski MM: Inhibition of autophagy in microglia and macrophages exacerbates innate immune responses and worsens brain injury outcomes. Autophagy 19: 2026-2044, 2023.
60. Zhao Y, Hao C, Bao L, Wang D, Li Y, Qu Y, Ding M, Zhao A and Yao W: Silica particles disorganize the polarization of pulmonary macrophages in mice. Ecotoxicol Environ Saf 193: 110364, 2020.
61. Xu T, Yan W, Wu Q, Xu Q, Yuan J, Li Y, Li P, Pan H and Ni C: MiR-326 inhibits inflammation and promotes autophagy in Silica-Induced pulmonary fibrosis through targeting TNFSF14 and PTBP1. Chem Res Toxicol 32: 2192-2203, 2019.
62. Grazioli S, Gil S, An D, Kajikawa O, Farnand AW, Hanson JF, Birkland T, Chen P, Duffield J, Schnapp LM, *et al*: CYR61 (CCN1) overexpression induces lung injury in mice. Am J Physiol Lung Cell Mol Physiol 308: L759-L765, 2015.
63. Whitsett JA: Airway epithelial differentiation and mucociliary clearance. Ann Am Thorac Soc 15 (Suppl 3): S143-S148, 2018.
64. Kim SH, Pei QM, Jiang P, Liu J, Sun RF, Qian XJ and Liu JB: Upregulation of MUC5AC by VEGF in human primary bronchial epithelial cells: Implications for asthma. Respir Res 20: 282, 2019.
65. Chen G, Ribeiro CMP, Sun L, Okuda K, Kato T, Gilmore RC, Martino MB, Dang H, Abzhanova A, Lin JM, *et al*: XBP1S Regulates MUC5B in a promoter Variant-Dependent pathway in idiopathic pulmonary fibrosis airway epithelia. Am J Respir Crit Care Med 200: 220-234, 2019.
66. Kim E, Mathai SK, Stancil IT, Ma X, Hernandez-Gutierrez A, Becerra JN, Marrero-Torres E, Hennessy CE, Hatakka K, Wartchow EP, *et al*: Aberrant multiciliogenesis in idiopathic pulmonary fibrosis. Am J Respir Cell Mol Biol 67: 188-200, 2022.

67. Dobrinskikh E, Estrella AM, Hennessy CE, Hara N, Schwarz MI, Kurche JS, Yang IV and Schwartz DA: Genes, other than Muc5b, play a role in bleomycin-induced lung fibrosis. Am J Physiol Lung Cell Mol Physiol 321: L440-Ll450, 2021.
68. Ma J, Rubin BK and Voynow JA: Mucins, mucus, and goblet cells. Chest 154: 169-176, 2018.
69. Singanayagam A, Footitt J, Marczynski M, Radicioni G, Cross MT, Finney LJ, Trujillo-Torralbo MB, Calderazzo M, Zhu J, Aniscenko J, *et al*: Airway mucins promote immunopathology in virus-exacerbated chronic obstructive pulmonary disease. J Clin Invest 132: e120901, 2022.
70. Koeppen M, McNamee EN, Brodsky KS, Aherne CM, Faigle M, Downey GP, Colgan SP, Evans CM, Schwartz DA and Eltzschig HK: Detrimental role of the airway mucin Muc5ac during ventilator-induced lung injury. Mucosal Immunol 6: 762-775, 2013.
71. Evans CM, Raclawska DS, Ttofali F, Liptzin DR, Fletcher AA, Harper DN, McGing MA, McElwee MM, Williams OW, Sanchez E, *et al*: The polymeric mucin Muc5ac is required for allergic airway hyperreactivity. Nature Commun 6: 6281, 2015.
72. Keith JD, Henderson AG, Fernandez-Petty CM, Davis JM, Oden AM and Birket SE: Muc5b contributes to mucus abnormality in rat models of cystic fibrosis. Front Physiol 13: 884166, 2022.
73. Hancock LA, Hennessy CE, Solomon GM, Dobrinskikh E, Estrella A, Hara N, Hill DB, Kissner WJ, Markovetz MR, Grove Villalon DE, *et al*: Muc5b overexpression causes mucociliary dysfunction and enhances lung fibrosis in mice. Nature Commun 9: 5363, 2018.
74. Danopoulos S, Alonso I, Thornton ME, Grubbs BH, Bellusci S, Warburton D and Al Alam D: Human lung branching morphogenesis is orchestrated by the spatiotemporal distribution of ACTA2, SOX2, and SOX9. Am J Physiol Lung Cell Mol Physiol 314: L144-Ll149, 2018.
75. Gajjala PR, Kasam RK, Soundararajan D, Sinner D, Huang SK, Jegga AG and Madala SK: Dysregulated overexpression of Sox9 induces fibroblast activation in pulmonary fibrosis. JCI Insight 6: e152503, 2021.
76. Danopoulos S, Thornton ME, Grubbs BH, Frey MR, Warburton D, Bellusci S and Al Alam D: Discordant roles for FGF ligands in lung branching morphogenesis between human and mouse. J Pathol 247: 254-265, 2019.
77. Basil MC and Morrisey EE: BASC-ing in the glow: Bronchioalveolar stem cells get their place in the lung. EMBO J 38: e102344, 2019.
78. Aros CJ, Vijayaraj P, Pantoja CJ, Bisht B, Meneses LK, Sandlin JM, Tse JA, Chen MW, Purkayastha A, Shia DW, *et al*: Distinct spatiotemporally dynamic Wnt-secreting niches regulate proximal airway regeneration and aging. Cell Stem Cell 27: 413-429.e4, 2020.
79. Sivakumar A and Frank DB: Paradigms that define lung epithelial progenitor cell fate in development and regeneration. Curr Stem Cell Rep 5: 133-144, 2019.
80. Rock J and Königshoff M: Endogenous lung regeneration: Potential and limitations. Am J Respir Crit Care Med 186: 1213-1219, 2012.
81. Chanda D, Otoupalova E, Smith SR, Volckaert T, De Langhe SP and Thannickal VJ: Developmental pathways in the pathogenesis of lung fibrosis. Mol Aspects Med 65: 56-69, 2019.
82. Deng M, Li J, Gan Y, Chen Y and Chen P: Changes in the number of CD31-CD45-Sca-1+ cells and Shh signaling pathway involvement in the lungs of mice with emphysema and relevant effects of acute adenovirus infection. Int J Chron Obstruct Pulmon Dis 12: 861-872, 2017.
83. Lau CI, Yánez DC, Papaioannou E, Ross S and Crompton T: Sonic Hedgehog signalling in the regulation of barrier tissue homeostasis and inflammation. FEBS J 289: 8050-8061, 2022.
84. Peng T, Frank DB, Kadzik RS, Morley MP, Rathi KS, Wang T, Zhou S, Cheng L, Lu MM and Morrisey EE: Hedgehog actively maintains adult lung quiescence and regulates repair and regeneration. Nature 526: 578-582, 2015.
85. Beachy PA, Karhadkar SS and Berman DM: Tissue repair and stem cell renewal in carcinogenesis. Nature 432: 324-331, 2004.
86. Chen X, Jin Y, Hou X, Liu F and Wang Y: Sonic hedgehog signaling: Evidence for its protective role in endotoxin induced acute lung injury in mouse model. PLoS One 10: e0140886, 2015.
87. Hu HH, Cao G, Wu XQ, Vaziri ND and Zhao YY: Wnt signaling pathway in aging-related tissue fibrosis and therapies. Ageing Res Rev 60: 101063, 2020.
88. Lehmann M, Hu Q, Hu Y, Hafner K, Costa R, van den Berg A and Königshoff M: Chronic WNT/β-catenin signaling induces cellular senescence in lung epithelial cells. Cellular Signal 70: 109588, 2020.